European Polymer Journal 46 (2010) 1334–1344

Contents lists available at ScienceDirect

European Polymer Journal

journal homepage: www.elsevier.com/locate/europolj

Effect of sequence distribution on the isothermal crystallization kinetics and successive self-nucleation and annealing (SSA) behavior of poly(ε-caprolactone-*co*-ε-caprolactam) copolymers

Rose Mary Michell [a], Alejandro J. Müller [a,*], Gaëlle Deshayes [b], Philippe Dubois [b]

[a] *Grupo de Polímeros USB, Departamento de Ciencia de los Materiales, Universidad Simón Bolívar, Apartado 89000, Caracas 1080-A, Venezuela*
[b] *Laboratory of Polymeric and Composite Materials, Center of Innovation and Research in Materials & Polymers (CIRMAP), University of Mons-UMONS, Place du Parc 20, Mons B-7000, Belgium*

ARTICLE INFO

Article history:
Received 14 January 2010
Received in revised form 13 March 2010
Accepted 16 March 2010
Available online 25 March 2010

Keywords:
Random copolymers
Block copolymers
SSA
Isothermal crystallization kinetics
Confined crystallization

ABSTRACT

Two types of miscible poly(ε-caprolactone-*co*-ε-caprolactam) copolymers were studied. In both cases catalyzed hydrolytic ring-opening polymerization was employed. For the first type, the comonomers were added simultaneously to obtain random copolymers. For the second type, the comonomers were added sequentially to obtain block copolymers. Successive self-nucleation and annealing (SSA) and isothermal crystallization studies were performed to both types of copolymers. The SSA results reflect the differences in molecular microstructure: block versus random copolymers. In a wide composition range only the polycaprolactam sequences were capable of crystallization in the random copolymers. Avrami indexes of approximately 3–4 were obtained corresponding to the spherulitic crystallization of these units within the copolymers. The block copolymer samples experienced a relatively small reduction of crystallization kinetics with composition, and this was attributed to the dilution effect caused by the miscible non-crystalline polycaprolactone units. On the other hand, for the random copolymers, the rate of crystallization strongly increased with polycaprolactam content while the energy barrier for secondary nucleation decreased exponentially. The comparison between miscible block and random copolymers provides a unique opportunity to distinguish the dilution effect of the polycaprolactone units (a moderate effect) on the isothermal crystallization and melting of the polyamide phase from the molecular microstructural effect in the random copolymers case (a dramatically strong effect), where the polycaprolactam sequences are interrupted statistically by polycaprolactone sequences.

© 2010 Elsevier Ltd. All rights reserved.

1. Introduction

Efforts at world-wide level are being made to decrease the amount of solid waste that is thrown in the environment, in particular, polymeric materials represent an important challenge since they remain a long time in the sanitary fillings and many are not transformed into biomass. As answer to this serious situation is the use of new polymeric materials that can be biodegraded [1].

Poly(ε-caprolactone-*co*-ε-caprolactam) copolymers can be considered as new class of biodegradable polymers with many potential applications. These materials can have the high thermal resistance and mechanical properties of polycaprolactam and the capacity of biodegradation of polycaprolactone [2–4].

These copolymers have been synthesized through different techniques, anionic, interfacial, ring-opening, polycondensation, and transesterification reactions in the melt [2–8]. Nevertheless the study of these copolymers has been centered mainly in their synthesis, basic characterization and degradation with one recent exception [9].

* Corresponding author. Fax: +58 2129063388.
E-mail address: amuller@usb.ve (A.J. Müller).

0014-3057/$ - see front matter © 2010 Elsevier Ltd. All rights reserved.
doi:10.1016/j.eurpolymj.2010.03.013

Most previous publications have reported the miscibility of the CLa and CLo-based sequences within the copolymers. Such miscibility has been confirmed by small angle X-ray scattering (SAXS) since no structure has been detected in the melt in the case of block or random copolymers [9]. In most studies, differential scanning calorimetry (DSC) results have also indicated that the copolymers are miscible. In most cases, only the polyamide component can crystallize and its melting temperature is a function of composition. Only one glass transition temperature has been detected for all the copolymers prepared and its value is also a function of composition, as expected for a miscible system [5–7,9,10]. Recent TEM studies [9], on the same block copolymers employed in this work, showed that a crystalline lamellar morphology was obtained regardless of composition, a typical feature of melt mixed crystallizable block copolymers [11–15].

The synthesis, morphology and thermal characterization of the copolymers employed here have been recently reported by some of us [4,16]. Two types of poly(ε-caprolactone (CLo))-*co*-poly(ε-caprolactam (CLa)) copolymers were prepared by catalyzed hydrolytic ring-opening polymerization. In order to prepare random copolymers, both cyclic comonomers were added simultaneously in the reaction medium for the first type of materials. ^{1}H and ^{13}C NMR demonstrated that the sequences of both types of repeating units were distributed randomly. For the second type of copolymers, the cyclic comonomers were added sequentially yielding diblock polyesteramides. DSC and WAXS demonstrated that in a wide composition range (CLo contents from 6% to 55%), only the CLa units were capable of crystallization in the random copolymers. Additionally, according to WAXS results, in one sample where both sequences were able to crystallize, we found no evidence of cocrystallization (i.e., the CLo and the CLa units always crystallized separately). The block copolymer samples experience a small reduction of crystallization and melting temperature with composition, which was attributed to the dilution effect caused by the miscible non-crystalline CLo units. On the other hand, the random copolymer samples experienced a dependence of their thermal transitions with composition. Such results were explained by the chemical composition effect in the random copolymers, where the CLa sequences are interrupted statistically by the CLo units making the crystallization of the polyamide strongly composition dependent. The enzymatic degradation of the copolymers in composted soil was also reported and the results obtained indicate a synergistic behavior where much faster degradation was produced in the random copolymers with a CLo content larger than 30% than in neat PCL [9].

In this paper, we present for the first time the isothermal crystallization kinetics of random and block copolymers of poly(ε-caprolactone-*co*-ε-caprolactam). The comparison of such results offers a unique opportunity to assess quantitatively the differences between the dilution effect caused by miscibility and the chemical constituent effect caused by the interruption of crystallizable units by a different comonomer. Additionally, we present results on the thermal fractionation of representative random and block copolymers of poly(ε-caprolactone-*co*-ε-caprolactam) employing the now well-known successive self-nucleation and annealing (SSA) technique [17–22].

2. Experimental part

2.1. Materials

The copolymers were obtained by the catalyzed hydrolytic ring-opening polymerization in bulk of ε-caprolactone (CLo) and ε-caprolactam (CLa), added simultaneously for the case of random copolymers and sequentially in the case of block copolymers. The details of the polymerizations and their mechanisms can be found elsewhere [4,9]. Table 1 shows the basic characteristics of the copolymers prepared. The nomenclature used for the copolymers employed here is the following: $C_{xx} - m - A_{yy}^{zz}$, where the numbers *xx* and *yy* represent the weight fraction of the units of CLo and CLa, respectively, *zz* indicates the number average molecular weight in kg/mol for the entire copolymer and the letter *m* indicates the microstructure of the copolymer, i.e., if it is a block copolymer the letter *b* is used and if it is a random copolymer, the abbreviation *ran* is employed.

2.2. Thermal analysis

The copolymers were analyzed using a Perkin-Elmer Pyris 1 calorimeter, with an inert atmosphere of ultra high purity nitrogen; it was calibrated with indium and tin. The weight of each sample was approximately 5 mg and the scanning rate used for the standard tests was 20 °C/min (both in cooling and heating). In all cases, the thermal history was erased by keeping the sample in the melt (usually at 20 °C above its peak melting temperature) for 3 min.

2.3. Isothermal crystallization

After erasing thermal history, the samples were cooled from the melt at 60 °C/min to the desired crystallization temperature. The evolution of the crystallization exotherm was followed as a function of time until saturation was

Table 1
Molecular characteristics of poly(ε-caprolactone-*co*-ε-caprolactam) copolymers.

Nomenclature	Type	M_n (g/mol)	CLo (wt%)	CLa (wt%)	Initiator[a]
PCL^{50}	Homopolymer	50,000	100		–
$PA6^{18.5}$	Homopolymer	18,500		100	–
$A_{100}{}^{6.7}$	Homopolymer	6700		100	Jeff M1
C_{52}-*b*-$A_{48}{}^{6.7}$	Block	6700	52	48	Jeff M1
C_{12}-*b*-$A_{88}{}^{24}$	Block	24,000	12	88	Jeff M1
C_{55}-*ran*-$A_{45}{}^{6.5}$	Random	6500	55	45	Jeff M1
C_{39}-*ran*-$A_{61}{}^{8.6}$	Random	8600	39	61	Jeff M1
C_{6}-*ran*-$A_{94}{}^{18.4}$	Random	18,400	6	94	Jeff M1
C_{23}-*ran*-$A_{77}{}^{26.2}$	Random	26,200	23	77	Jeff M1
C_{36}-*ran*-$A_{64}{}^{31.8}$	Random	31,800	36	64	Jeff M1
C_{46}-*ran*-$A_{54}{}^{38}$	Random	38,000	46	54	Jeff M1
C_{8}-*ran*-$A_{92}{}^{30.5}$	Random	30,500	8	92	Jeff ED
C_{36}-*ran*-$A_{64}{}^{64.6}$	Random	64,600	36	64	Jeff ED

[a] Macroinitiator, Jeff M1 is NH_2-monofunctional and Jeff ED is NH_2-bifunctional.

reached (at approximately three times the half-crystallization time). Then the sample was heated at 20 °C/min in order to record the melting behavior of the isothermally crystallized copolymer. In order to determine the suitable crystallization temperatures (T_c), previous tests were made. The sample was cooled from the melt at 60 °C/min to a pre-established T_c and then it was immediately heated at 20 °C/min in order to see if any melting could be detected. If an endotherm was recorded, then the T_c employed was too low, since some crystallization occurred during the cooling to T_c at 60 °C/min. Then a test was performed with a higher T_c until no crystallization occurs during the previous cooling. A T_c range of at least 7 different temperatures was employed (usually separated by 1 °C difference) [23].

2.4. Isothermal step crystallization [24]

In cases where slow crystallization kinetics are encountered, conventional isothermal kinetics can be beyond the resolution of the DSC (i.e., the amount of heat evolved per unit time is too small to be measured isothermally). In that case, we employed the "isothermal step crystallization" method. This method has been employed for the first time by us in Ref. [24].

The method consists of the following steps:

(a) Erasure of thermal history by heating the sample to a suitable temperature and holding it at that temperature for 3 min.
(b) Fast cooling (60 °C/min) from the melt down to T_c. To select the lowest T_c employed, we performed immediate heating scans after the corresponding cooling scans to T_c in order to corroborate that crystallization did not occur during the cooling process to T_c.
(c) The sample is held at T_c for a time t_c, which is later increased in the subsequent steps.
(d) Heating at 20 °C/min from T_c to a temperature where the sample is fully melted. The heat of fusion calculated from this DSC heating scan must correspond to the crystallization enthalpy of the crystals formed during step "c" at T_c for the specified crystallization time (t_c).
(e) Steps (a–d) are repeated employing the same T_c in step "b", but at increasing t_c. The last t_c was taken as the time the melting enthalpy in the subsequent heating scan did not change with respect to the previous one.
(f) The whole process is repeated for 6 different T_c temperatures.

2.5. Successive self-nucleation and annealing (SSA) [17–22]

Samples with approximately 3.3 mg were employed to perform the SSA tests. Detailed procedure can be found elsewhere [17–22]. After erasing thermal history, the samples were cooled from the melt at 30 °C/min in order to produce a standard thermal history. Then the samples were heated at 30 °C/min until the first T_s temperature, or self-seeding temperature was reached. The fractionation time, or holding time at T_s was always constant at 5 min. After 5 min had elapsed, the samples were cooled at 30 °C/min down to a low enough temperature to allow crystallization (30 °C for homopolymers and −30 °C for copolymers). Then the sample was heated once more at 30 °C/min but this time up to a T_s temperature that was 10 °C lower than the first one. This means that the fractionation window employed was 10 °C, i.e., T_s temperatures separated by 10 °C were employed during the heating and cooling cycles. The whole process was repeated until the full melting range of the polymer was covered and then a final heating scan is performed to melt all the produced thermal fractions.

3. Results and discussion

3.1. Successive self-nucleation and annealing (SSA)

The SSA technique is a powerful tool to perform thermal fractionation in a fast and simple way. The technique is particularly sensitive to any interruption on the crystallizable linear sequences of a polymer. For this reason it has been extensively used to characterize ethylene/α-olefin copolymers. In such materials, SSA can yield information on the short chain branching content and distribution along the ethylene chain [17–22].

In case of random copolymers, when the major component is capable of crystallization, the second component will interrupt the crystallizable sequences and therefore these materials should also be sensitive to thermal fractionation [21,22].

Fig. 1 shows the final DSC heating scan after applying the SSA technique to two polyamides. The first sample was synthesized in our laboratory, employing similar techniques to those employed for the copolymers (e.g., $A_{100}^{6.7}$) and the second sample is a commercial PA6 (e.g., $PA6^{18.5}$). In linear homopolymers the SSA technique is usually less sensitive, since the only possible thermal fractionation that can be achieved is due to molecular segregation due to differences in chain length. In the case of polyamides, the fact that they have usually very low melt viscosity probably helps achieving a certain degree of thermal fractionation in spite of the absence of branches or any other chemical defects that can interrupt the crystallizable chain. Similar fractionation of linear chain polymers has been reported previously by us in poly(ε-caprolactone) [25] and in poly(p-dioxanone) [26]. The DSC scans in Fig. 1 show the appearance of multiple endotherms. Each endotherm corresponds to the melting of a particular lamellar size population. The higher the melting point is, the thicker the lamellae are. In the homopolymer case, the thickest lamellae are constituted by the longest chains within the distribution [27,28]. The distribution of melting points exhibited by both polyamide homopolymers indicates that a monomodal distribution of chain lengths is present in both cases, an expected result for linear polyamides.

A comparison between the commercial polyamide and the synthesized in the laboratory can be made, see Fig. 1. In the commercial PA6, the number of thermal fractions is higher and they are better defined than in the laboratory one. This observation is consistent with the nature of the

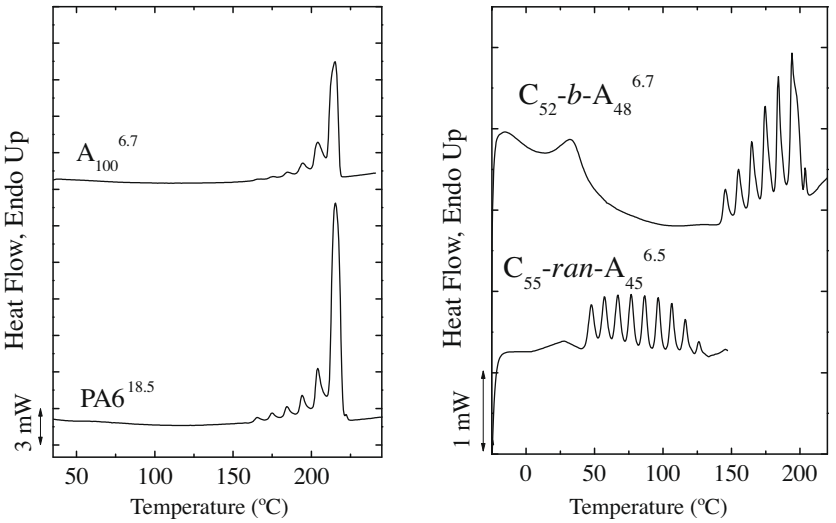

Fig. 1. Final heating DSC scan after applying the SSA protocol. Left: a commercial polyamide sample ($PA6^{18.5}$) and a sample synthesized with similar techniques to those employed for the preparation of the copolymers ($A_{100}{}^{6.7}$). Right: the indicated random and block copolymer samples.

polymers in question, since the commercial PA6 has a broader distribution of molecular weights. The polyamide synthesized in the laboratory has a narrow and monomodal distribution of molecular weights and will be more difficult to fractionate [4].

Fig. 1 also presents the SSA results for two representative copolymers of nearly the same composition but different chemical structure (i.e., random versus blocky nature). In the case of these copolymers, the thermal fractionation is the product of two effects: the distribution of molecular weights and the distribution of the crystallizable linear sequences, in this case, the CLa linear and uninterrupted sequences. Both copolymers exhibit several endothermal peaks with better definition than in the homopolymers case, this indicates that the copolymers are easier to fractionate than the homopolymers, and as a result the lamellar populations are more differentiated.

The SSA results are fully consistent with the differences in the distribution of the CLo sequences expected between a random and a block copolymer. Because the crystallizable CLa sequences are frequently interrupted in the random copolymer, the development of thicker lamellae is hindered, therefore, a very wide range of thermal fractions is generated that melt at substantially lower temperatures than in the homopolymer or in the block copolymer case. The block copolymer case is interesting because the CLo sequences will not interrupt the crystallizable CLa units; however, because of the miscibility between the two components, there is a melting point depression in the fractions generated when compared with the PA6 homopolymer. The melting peak at temperatures in between 25 and 50 °C corresponds to the fusion of the CLo sequences crystals that are able to form in the block copolymer, but not in the random one (previous studies employing WAXS demonstrated that for all the random copolymers examined here, only the CLa units are able to crystallize). The reason behind the better fractionation in the block copolymer case as compared to the homopolymer is the increased molecular mobility provided by the plasticizing action of the CLo sequences. There are also some changes in the distributions of melting points generated that can be expected on the basis of the chemically different constitution of the random and block copolymers, however, they are both monomodal as expected.

In summary, the SSA technique has confirmed previous NMR results regarding the nature of the copolymers involved: random versus block copolymers. Even more interesting, the comparison between samples with nearly identical CLa content but in a widely different distribution along the chain allows us to separate the effects of miscibility from that of chemical microstructure. The effect of miscibility alone is present in the block copolymer case, which basically causes moderate melting point depression and enhanced molecular mobility to produce better fractionation in comparison to the homopolymer. The effect of miscibility superimposed to the much more dramatic effect of chemical microstructure is present in the random copolymer case, where the frequent interruption (in a random fashion) of the CLa crystallizable sequences leads to extreme depressions in the melting points of the produced fractions.

3.2. Isothermal crystallization

3.2.1. Equilibrium melting temperature determination

As indicated in Section 2, the samples were isothermally crystallized and immediately heated to record their melting behavior. A representative example of such DSC heating scans can be seen in Fig. 2(a) for the C_{23}-*ran*-$A_{77}{}^{26.7}$ random copolymer. Two melting peaks were observed for the different isothermal crystallization temperatures employed. Fig. 2(b) shows a typical Hoffman–Weeks plot for the data of Fig. 2(a). It can be seen that both melting peaks have a dependence with T_c, a fact that rules out one possible explanation for their origin. If the double peak was due to melting and recrystallization, one peak would normally be invariant

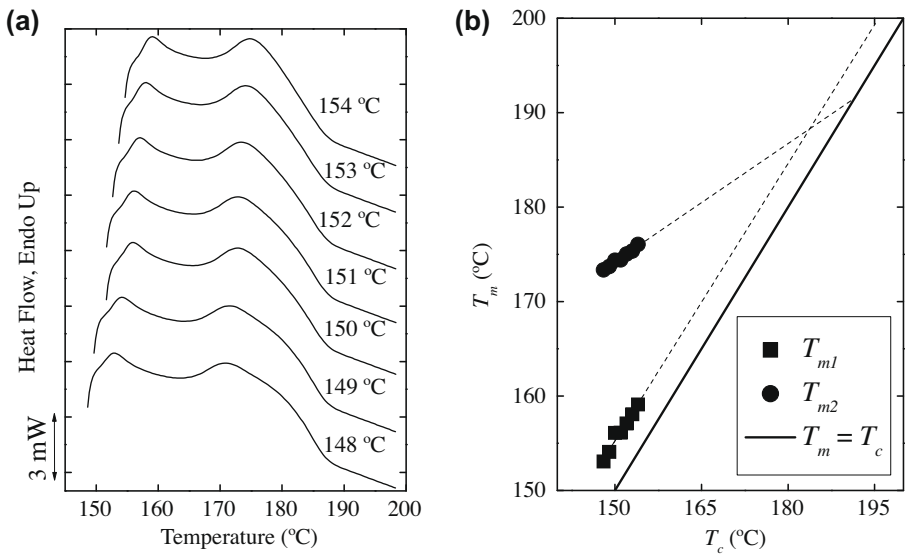

Fig. 2. (a) DSC heating scans after isothermal crystallization at the indicated temperatures for the C_{23}-*ran*-$A_{77}^{26.7}$ random copolymer. (b) Hoffman–Weeks plot for the same copolymer.

with T_c, and this is not the case here. The lower temperature melting peak is probably due to the melting of the crystals generated during secondary crystallization. The higher temperature melting peak is most probably due to the fusion of the crystals generated during primary isothermal crystallization temperature. This explanation is also consistent with the literature [29,30] and with the fact that only the second melting peak (higher temperature one) can be successfully extrapolated to yield a value of the equilibrium melting point, as indicated in Fig. 2(b).

A few exceptions to the above mentioned behavior were encountered. In the case of the C_{12}-*b*-A_{88}^{24} block copolymer and the PA6 homopolymer three melting peaks were observed. In those two cases, the final melting peak was clearly the product of recrystallization during the scan since its melting temperature was independent of T_c. The second melting point (at intermediate temperatures in these two cases) did depend on T_c and was used to calculate the equilibrium melting point by the Hoffman–Weeks extrapolation procedure.

The equilibrium melting point or T_m^0 is the melting temperature of an ideal crystal, that is, the fusion temperature of an infinite stack of extended chain crystals [32].

This temperature is affected by factors like the molecular weight, the distribution of defects along the chain, miscibility and the distribution of comonomer in the case of a copolymer [28,29]. Table 2 shows the values of the equilibrium melting temperatures obtained for all the samples employed. In spite of some exceptions caused by errors in the extrapolation procedure and data scattering, a general trend emerges at least for the random copolymer case. In the random copolymer case, the T_m^0 values decrease sharply as the amount of CLo sequences incorporated in the chains increases, as expected. A T_m^0 reduction was also obtained for the two block copolymer samples employed, its value also decreased with CLo incorporation. No large differences were obtained in this case in between the random and the block copolymer cases, a fact that may be due to the large errors involved in the Hoffman–Weeks extrapolation procedure. The application of the Hoffman–Weeks method in the case of copolymers has been questioned by Mandelkern [29].

3.2.2. Isothermal crystallization kinetics

An experimentally determined measure of the overall crystallization rate (that includes nucleation and growth) is that given in a DSC isothermal crystallization experiment by the inverse of the half-crystallization time. The half-crystallization time is the time needed for the 50% relative transformation to the semi-crystalline state. The data is normalized with respect to the maximum latent heat of crystallization that can be achieved by the sample in question [23].

Fig. 3 presents experimental data of the overall crystallization rate of the polyamide component (with one exception, PCL) as a function of the isothermal crystallization temperature T_c. The overall crystallization rate is a clear function of the CLa content within the copolymers, however an important difference is observed in between the random and the block copolymers. As the amount of CLo units increases, the supercooling needed for crystallization also increases, or in other words we need to decrease T_c in order to provoke crystallization. The decrease in T_c is much larger for the random copolymers than for the block copolymers of similar CLa contents. This result was expected on the basis of our previous work that examined non-isothermal crystallization of these samples [9] and on the basis of the SSA results presented above. Once again we can rationalize the results by considering that in the block copolymers, the miscibility is the only cause of the moderate crystallization rate depression as compared to the homopolymer. However, in the case of the random

Table 2
Variation of T_m^0 with the content of caprolactam for the poly(ε-caprolactone-*co*-ε-caprolactam) block and random copolymers.

Sample	% CLa	T_m^0 (°C) H–W	T_m^0 (°C) [31]
PCL^{50}	0	64	69
$PA6^{18.5}$	100	290	260
C_{12}-*b*-$A_{88}{}^{24}$	88	217	
C_{55}-*b*-$A_{46}{}^{6.5}$	52	204	
C_6-*ran*-$A_{94}{}^{18.4}$	94	263	
C_8-*ran*-$A_{92}{}^{30.5}$	92	221	
C_{23}-*ran*-$A_{77}{}^{26.2}$	77	192	
C_{36}-*ran*-$A_{64}{}^{31.8}$	64	175	
C_{36}-*ran*-$A_{64}{}^{64.6}$	64	186	
C_{39}-*ran*-$A_{61}{}^{8.6}$	61	170	
C_{46}-*ran*-$A_{54}{}^{38}$	54	180	
C_{55}-*ran*-$A_{45}{}^{6.5}$	45	210	

copolymers, the molecular microstructure is provoking a much larger effect as the crystallizing CLa sequences are frequently interrupted by the CLo units.

Another way to examine the results presented in Fig. 3 is to choose a constant value of $1/\tau_{1/2}$ (for instance 0.5 s^{-1}) and plot the crystallization temperature needed to achieve that constant overall crystallization rate. Such a plot is presented in Fig. 4 and the very large difference between the random and the block copolymer samples is very clear, since the former ones display a dramatic reduction in T_c as the CLa content is decreased while the block copolymers only experienced a small reduction as compared to the homopolymer value.

The experimental data gathered and partially presented in Fig. 3 can also be fitted to isothermal crystallization theories. One of the most popular theories to model isothermal crystallization kinetics employing overall crystallization rate data (i.e., data that includes nucleation and growth measurements, like those performed by DSC) is that due to Avrami. In this paper, we have closely followed the experimental procedures and analysis established previously by Lorenzo et al. [23]. The Avrami equation can be expressed as [23,33]:

$$1 - V_c(t - t_0) = \exp(-k(t - t_0)^n) \tag{3.1}$$

where V_c is the relative volumetric transformed fraction, t is the experimental time, t_0 is the induction time (time needed for the first exothermal signal to be registered on the DSC) n is the Avrami index and k is the overall crystallization rate constant (i.e., it contains contributions from both nucleation and growth) [22,34].

We have employed the Avrami theory to fit the isothermal DSC data in a conversion range of approximately 3–20%, this corresponds to the primary crystallization range where the Avrami analysis is most adequate. In such a range the correlation coefficients of the fit are always in excess of 0.99 (see Table 3). In order to illustrate the fitted range, two examples are provided: the polyamide homopolymer and two copolymers of similar composition, one random and one block. Fig. 5 shows how the Avrami fit (solid line) represents very well the experimental data almost up to 50% conversion. Fig. 6 on the other hand shows the Avrami derived DSC curve as compared to the experimental data, and once again the fit is excellent on the left hand side of the DSC curve, or within the primary crystallization range (i.e., before spherulites impinge on one another and the DSC curve goes through a minimum value). For details on how Figs. 5 and 6 were obtained please check out Ref. [23].

Table 3 shows the values obtained from the Avrami fit: the parameters K, n and the predicted half-crystallization time as compared to the experimental value. The values of K, the overall crystallization rate constant follow a trend that resembles that of $1/\tau_{1/2}$ already presented in Fig. 3. The values of $1/\tau_{1/2}$ predicted by the Avrami fit as very close to the experimental one in most cases, as expected from the trends exemplified in Fig. 5, as the Avrami theory fits mostly the primary crystallization range.

The value of n is associated to the nucleation type present during the experiment (e.g., sporadic or instantaneous) and also to the dimension of the supercrystalline structures formed (in the case of polymers usually spherulites are formed and occasionally axialites or other type or lower dimension aggregates) [11,29].

Fig. 7 displays the values of the Avrami index obtained as a function of crystallization temperature for all the samples examined. The results refer to the isothermal

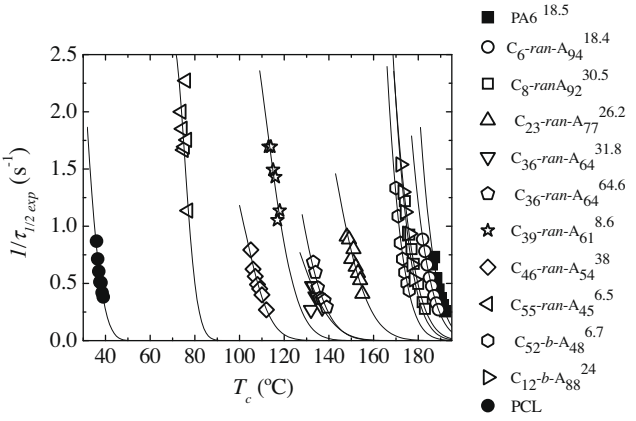

Fig. 3. Values of the inverse of $\tau_{1/2}$ as a function of the isothermal crystallization temperature for the different poly(ε-caprolactone-*co*-ε-caprolactam) block and random copolymers.

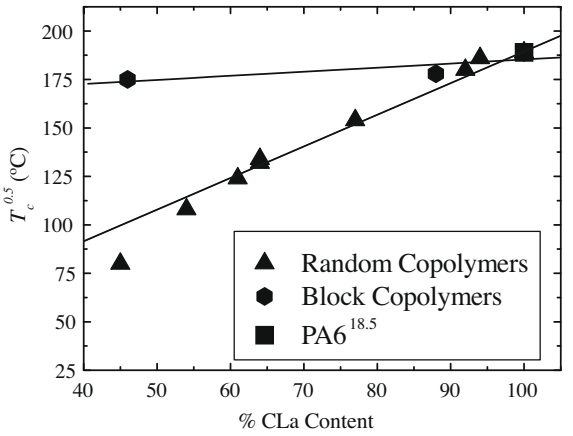

Fig. 4. Isothermal crystallization temperature needed to obtain a constant value of $1/\tau_{1/2}$ of 0.5 s^{-1} as a function of CLa content for the indicated samples.

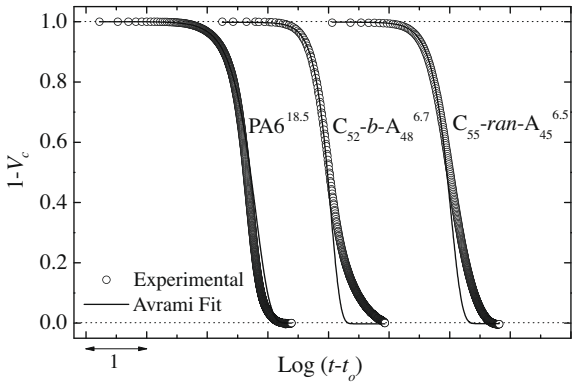

Fig. 5. Variation of $1 - V_c$ (volumetric relative amorphous content) with $\log(t - t_0)$. A comparison between the experimental data and the fitting of the Avrami equation for the indicated samples. The crystallization temperatures were 193, 172 and 82 °C for the PA6$^{18.5}$, C_{52}-b-$A_{48}$$^{6.7}$ and C_{55}-ran-$A_{45}$$^{6.5}$, respectively.

Table 3
Avrami fitting parameters (n, K, $\tau_{theo}^{1/2}$) and their correlation coefficient R^2. The experimental value of $\tau^{1/2}$ is given for comparison purposes. The conversion range employed was the same in every case, 3–20%.

Sample	T (°C)	n	K (min^{-n})	$\tau_{theo}^{1/2}$ (min)	$\tau_{exp}^{1/2}$ (min)	R^2	Sample	T (°C)	n	K (min^{-n})	$\tau_{theo}^{1/2}$ (min)	$\tau_{exp}^{1/2}$ (min)	R^2
PA6	191.0	2.3	0.046	3.33	3.25	0.9998	C_{39}-ran-$A_{61}$$^{8.6}$	113.0	2.4	2.950	0.54	0.59	0.9995
	192.0	2.3	0.029	3.94	3.90	0.9999		114.0	2.4	2.990	0.55	0.59	0.9997
	192.5	2.5	0.022	4.03	3.87	0.9999		115.0	2.4	2.250	0.62	0.67	0.9994
	193.0	1.9	0.037	4.80	4.20	0.9992		116.0	2.3	1.880	0.65	0.70	0.9996
	193.5	1.8	0.033	5.17	4.47	0.9993		117.0	2.2	0.960	0.86	0.95	0.9995
	194.0	1.8	0.031	5.50	4.75	0.9990		118.0	2.3	1.140	0.80	0.88	0.9997
C_6-ran-$A_{94}$$^{18.4}$	182.0	3.2	0.723	0.99	1.13	0.9994	C_{46}-ran-A_{54}^{38}	105.0	2.3	0.590	1.07	1.26	0.9990
	183.0	3.2	0.449	1.14	1.28	0.9996		106.0	2.2	0.380	1.32	1.60	0.9988
	184.0	3.4	0.248	1.35	1.51	0.9995		107.0	2.4	0.280	1.44	1.78	0.9983
	185.0	3.8	0.111	1.62	1.82	0.9993		108.0	2.5	0.200	1.64	2.04	0.9984
	186.0	3.8	0.060	1.91	2.10	0.9995		109.0	2.3	0.170	1.83	2.21	0.9993
	187.0	4.2	0.021	2.31	2.55	0.9992		110.0	2.5	0.120	2.03	2.50	0.9986
C_8-ran-$A_{92}$$^{30.5}$	174.0	3.1	1.640	0.76	0.82	0.9999	C_{55}-ran-$A_{45}$$^{6.5}$	74.0	2.6	4.100	0.50	0.50	0.9998
	176.0	3.3	0.664	1.01	1.08	0.9999		74.5	2.5	3.300	0.53	0.54	1.0000
	177.0	3.4	0.406	1.17	1.25	1.0000		75.0	2.6	2.890	0.58	0.60	0.9998
	178.0	3.7	0.200	1.39	1.49	0.9999		75.5	2.5	2.850	0.57	0.59	0.9999
	180.0	3.9	0.058	1.90	2.08	0.9999		76.0	2.7	6.350	0.44	0.44	0.9998
	182.0	4.5	0.007	2.79	2.97	0.9995		76.5	2.6	3.130	0.56	0.57	0.9999
C_{23}-ran-$A_{77}$$^{26.2}$	148.0	2.7	0.754	0.97	1.10	0.9993	C_{12}-b-A_{88}^{24}	172.0	3.1	3.220	0.61	0.65	0.9975
	149.0	2.7	0.676	1.01	1.13	0.9996		173.0	3.2	1.920	0.73	0.77	0.9999
	150.0	3.0	0.366	1.24	1.40	0.9995		174.0	3.2	1.210	0.84	0.89	1.0000
	151.0	3.1	0.486	1.12	1.25	0.9996		175.0	3.5	0.680	1.01	1.07	0.9999
	152.0	3.1	0.258	1.37	1.55	0.9994		176.0	3.5	0.680	1.01	1.07	0.9999
	153.0	3.2	0.185	1.51	1.69	0.9994		177.0	3.8	0.200	1.40	1.50	0.9999
C_{36}-ran-$A_{64}$$^{31.8}$	132.0	1.5	0.150	2.82	3.73	0.9988	C_{52}-b-$A_{48}$$^{6.7}$	170.0	2.7	1.700	0.71	0.75	1.0000
	132.5	1.5	0.240	1.98	2.10	0.9999		171.0	2.8	1.000	0.88	0.92	1.0000
	133.0	1.6	0.250	1.94	2.12	1.0000		172.0	2.7	0.560	1.08	1.17	0.9999
	134.0	1.5	0.190	2.39	2.59	0.9999		173.0	3.0	0.340	1.27	1.40	0.9997
	135.0	1.5	0.170	2.59	2.67	0.9997		174.0	3.2	0.190	1.51	1.68	0.9995
	136.0	1.4	0.160	2.91	2.84	0.9998		175.0	3.1	0.110	1.81	2.00	0.9996
C_{36}-ran-$A_{64}$$^{64.6}$	133	1.4	0.46	1.33	1.46	0.9998	PCL	36.0	2.8	0.47	1.14	1.15	1.0000
	134	1.5	0.34	1.62	1.68	0.9999		36.5	2.9	0.28	1.38	1.40	1.0000
	135	1.4	0.24	2.08	2.17	1.0000		37.0	2.8	0.18	1.62	1.65	1.0000
	136	1.4	0.19	2.61	2.70	1.0000		37.5	2.7	0.12	1.92	1.95	0.9999
	137	1.3	0.18	2.87	2.76	0.9999		38.0	2.7	0.11	1.97	1.97	0.9998
	138	1.3	0.17	3.00	2.87	0.9999		38.5	2.6	0.07	2.38	2.38	0.9997

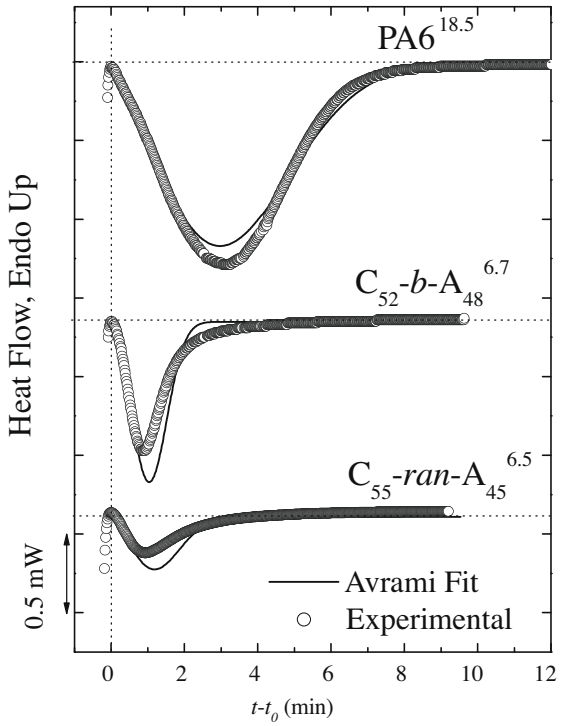

Fig. 6. Experimental DSC isotherms and simulated DSC curves by the Avrami equation for the PA6 homopolymer, and C_{52}-*b*-$A_{48}^{6.7}$ and C_{55}-*ran*-$A_{45}^{6.5}$ copolymers. The crystallization temperatures were 193, 172 and 82 °C for the $PA6^{18.5}$, C_{52}-*b*-$A_{48}^{6.7}$ and C_{55}-*ran*-$A_{45}^{6.5}$, respectively.

crystallization of the polyamide component, except in two cases: PCL and C_{52}-*b*-$A_{48}^{6.7}$ (CLo block).

In general, the polyamide component crystallization exhibits reasonable values of the Avrami index, since polarized optical microscopy observations (not shown here) indicated that most of the samples crystallized with spherulitic superstructures. Instantaneously nucleated spherulites should yield an Avrami index of 3 (experimental values of 2.5–3.4 are considered a good approximation), while sporadically nucleated spherulites should exhibit an Avrami index of 4 (values of 3.5–4.4 are also considered a good approximation). One exception to this general behavior was found for C_{36}-*ran*-$A_{64}^{31.8}$ and C_{36}-*ran*-$A_{64}^{64.6}$ since both materials exhibited a very high nucleation density (in polarized optical microscopy no definite features could be ascertained) and their Avrami indexes were close to 1.5, so it is believed that the CLa sequences crystallizes in axialites (2D structures) instantaneously nucleated.

For the C_{52}-*b*-$A_{48}^{6.7}$ block copolymer sample, both blocks were able to crystallize. Therefore, this is the only double crystalline diblock copolymer (see Ref. [13]) sample among those employed here. In this case, the CLa sequences always crystallizes first because of its much higher crystallization temperature. The CLa block forms spherulites at temperatures where the CLo block is molten. Upon further cooling, the CLo component is able to crystallize at much lower temperatures (see Fig. 7, the CLa component crystallizes at temperatures higher than 175 °C while the CLo component crystallizes at temperatures below 10 °C). The Avrami index found for the CLo block within this copolymer was extremely low, in the range 0.4–0.8. Avrami indexes in the order of 1 or lower indicate a dramatic change in the order of the crystallization kinetics (an Avrami index of 1 would be equivalent to a first order crystallization kinetics). Such a change can be observed in Fig. 6 where the shape of the crystallization isotherm changes from a typically sigmoidal shape encountered for the PCL homopolymer (the usual behavior in polymeric materials, where the Avrami index is typically larger than 2.5) to an exponential growth with time (closely resembling a first order process).

The reason why the crystallization kinetics changed so much has already been studied in a series of block copolymers [11–14] where confinement is the governing mechanism. In the present case, the CLo sequence has to crystallize within the interlamellar regions of the CLa block that has already formed spherulites. This leads to a confinement of the CLo sequence. In this situation, the nucleation is the rate determining step, since the crystallization is occurring at such large supercoolings that is virtually instantaneous. Another evidence that indicates that the CLo block is crystallizing in a confined fashion is its lower crystallization temperature as compared to the homopolymer sample. This increased supercooling could

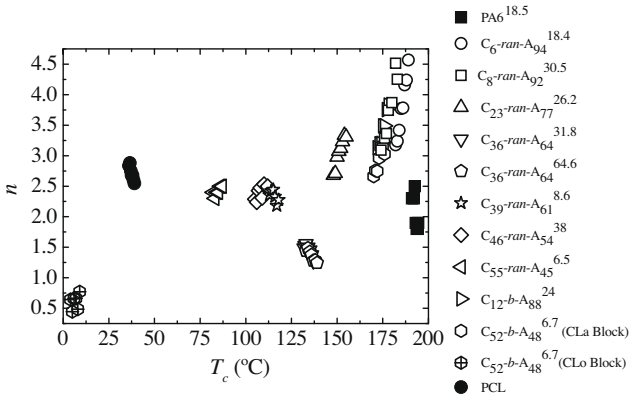

Fig. 7. Avrami index (n) versus isothermal crystallization temperature (T_c) for the indicated samples.

indicate that the nucleation is either homogeneous or nucleated by the interphases present in the system. A detailed explanation of the consequences of confinement on the crystallization kinetics can be found in two recent reviews [11,14].

The confined crystallization is usually encountered in strongly segregated block copolymers or in immiscible blends [11–14], however in this case we have been able to observe it in a miscible block copolymer system. Similar results have been reported recently for miscible mixtures with two crystallizable components, and in block copolymers with miscible blocks [13,34].

Even though the model of nucleation and growth proposed by Lauritzen and Hoffman (L–H model) has been under much criticism lately [28,29,35–39], it is still one of the few models that provides easy to use analytical expressions that are capable of fitting the experimental data very well (even though the physical meaning of some of the fitting parameters could be questionable) and therefore it is widely employed [40].

When the isothermal crystallization is determined by spherulitic growth experiments, the energy barrier determined by applying the L–H model refers exclusively to secondary nucleation or crystal growth. Instead, when the inverse of half-crystallization time ($1/\tau_{1/2}$) values obtained from DSC isothermal overall crystallization kinetic data is considered, both primary nucleation and crystal growth are considered. Therefore, the energetic parameters that we obtained after applying any classical kinetic crystallization theory to DSC data will include contributions from both processes (Fig. 8).

The general form of the L–H theory is given by Eq. (3.2) [40]:

$$G = G_0 \exp\left(-\frac{U^*}{R(T_c - T_\infty)}\right) \exp\left(-\frac{K_g}{T_c \Delta T f}\right) \quad (3.2)$$

where G is the rate of crystallization, U^* is the energy of activation for the transport of molecules to the growth front, R is the ideal gas constant, T_c is the isothermal crystallization temperature, T_∞ is the temperature to which all molecular movements stop, K_g is a nucleation constant that is proportional to the energy barrier for nucleation and growth (since in this case we will employ DSC data) ΔT is the supercooling ($T_m^0 - T_c$) and f is a correction factor ($f = 2T_c/(T_m^0 + T_c)$) [40,41]. In this work we employ as a measure of crystallization rate the values of $1/\tau_{1/2}$. The values employed for the L–H fitting are show in Table 4.

The data presented in Fig. 3 was fitted to the L–H theory and the fittings can be seen in Fig. 3 as the solid lines. The fittings were satisfactory in all cases yielding correlation coefficients in excess of 0.9. One of the most important parameters that can be obtained through the L–H treatment is K_g. This value was obtained and plotted as a function of CLa content in Fig. 9. A large difference was found in the trends corresponding to the diblock copolymers versus the random copolymers. For the diblock copolymers case, the value of K_g increases only slightly with CLo content in the copolymers as compared to PA6 homopolymer, the trend is described in Fig. 9 by a straight line. However, in the case of the random copolymers, the energy barrier for the overall crystallization increases exponentially with the content of CLo units. Once more the results are rationalized in terms of the differences in molecular microstructure between both types of copolymers as previously explained above.

4. Conclusions

In this work, we were able to compare miscible random and block copolymers composed of CLa and CLo sequences.

Table 4
Values of the different parameters employed for the L–H fitting for the PA6 homopolymer and the CLa sequences [42].

Parameter	Value
U^*	1430 cal/mol
T_∞ [a]	293.15 K
R	1.987 cal/mol K

[a] $T_\infty = T_g - 30$ K, T_g determined by DSC.

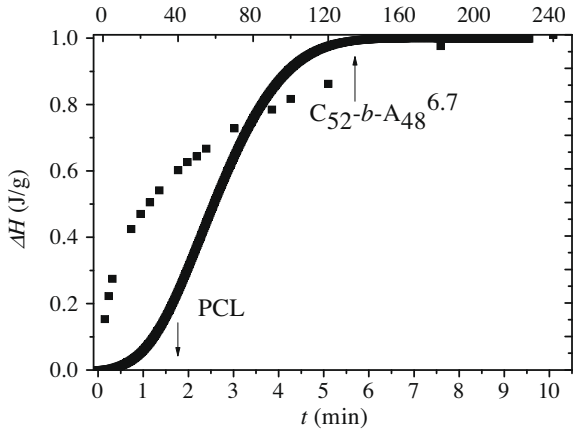

Fig. 8. Variation of the enthalpy of crystallization (ΔH_c) with time (t) for PCL and the PCL block within the C_{52}-b-$A_{48}^{6.7}$ copolymer.

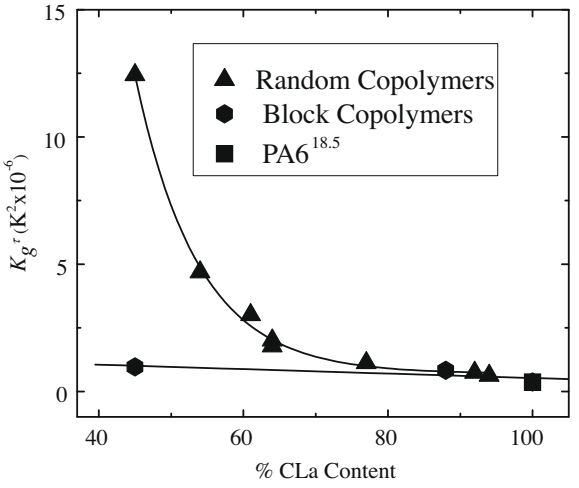

Fig. 9. Variation of K_g^τ with caprolactam content for the copolymers block and random poly(ε-caprolactone-*co*-ε-caprolactam) copolymers.

The SSA results clearly indicate the large differences in melting range derived from the widely different chemical microstructures. In the block copolymers case, a moderate melting point depression for the CLa component was detected in view of a dilution effect caused by the presence of the miscible CLo units. A much larger melting point depression was found in the random copolymer as a function of composition because of the frequent interruption of the linear crystallizable CLa sequences by the CLo units. However, for all copolymers the quality of the thermal fractionation was much improved as compared to the homopolymers because of the enhanced molecular mobility provided by the miscible CLo units on the CLa chains.

The isothermal crystallization kinetics results were completely consistent with the above explanation as the overall crystallization rate of the CLa sequences was found to be strongly dependent of composition for the random copolymers and only weakly composition dependent for the block copolymers. The energy barrier for overall crystallization also followed a similar trend since it was exponentially dependent on CLo units content while only weakly dependent on composition for the block copolymers. The Avrami parameters behaved as expected for most of the copolymer samples reflecting spherulitic or axialitic superstructures that were sporadically or instantaneously nucleated. In the particular case of a C_{52}-*b*-A_{48}[6.7] block copolymer, the CLo units were able to crystallize, as well as the CLa units, and their crystallization kinetics were followed by DSC sequentially. After the CLa units crystallized in spherulitic superstructures, at lower temperatures the CLo units crystallized in a confined fashion in the interlamellar spaces. Such confined crystallization produced a nearly first order crystallization kinetics (e.g., an Avrami index close to 1 was obtained).

Acknowledgements

The USB team would like to thank the "Decanato de Investigación y Desarrollo" (DID) for their generous funding through Grant DID-GID-G02. CIRMAP thanks the "Belgian Federal Government Office Policy of Science (SSTC)" for general support in the frame of the PAI-6/27.

References

[1] Zheng Y, Yanful EK. A review of plastic waste biodegradation. Crit Rev Biotechnol 2005;25(4):243–50.
[2] Draye AC, Persenaire O, Brozek J, Kosek J, Dubois P. Thermogravimetric analysis of poly(ε-caprolactone) and poly[(ε-caprolactam)-co-(ε-caprolactone)] polymers. Polymer 2001;42(20):8325–32.
[3] Gonsalves KE, Chen X, Cameron JA. Degradation of nonalternating poly(ester-amides). Macromolecules 1992;25(12):3309–12.
[4] Deshayes G, Delcourt C, Verbruggen I, Trouillet-Fonti L, Touraud V, Fleury E, et al. Activation of hydrolytic polymerization of ε-caprolactam by ester functions: straightforward route to aliphatic polyesteramides. React Funct Polym 2008;68(9):1392–407.
[5] Chromcová D, Bernásková A, Brozek J, Prokopová I, Roda J, Náhlík J, et al. Degradation of polyesteramides prepared by anionic polymerization of ε-caprolactam in the presence of poly(ε-caprolactone). Polym Degrad Stab 2005;90(3):546–54.
[6] Chromcová D, Baslerová L, Roda J, Brozek J. Polymerization of lactams. 99 preparation of polyesteramides by anionic copolymerization of ε-caprolactam and ε-caprolactone. Eur Polym J 2008;44(6):1733–42.
[7] Goodman I, Vachon RN. Copolyesteramides IV anionic copolymers of ε-caprolactam with ε-caprolactone molecular and chain structure. Eur Polym J 1984;20(6):529–37.
[8] Tokiwa Y, Suzuki T. Synthesis of copolyamide-esters and some aspects involved in their hydrolysis by lipase. J Appl Polym Sci 1979;24(7):1701–11.
[9] Michell RM, Müller AJ, Castelletto V, Hamley I, Deshayes G, Dubois P. Effect of sequence distribution on the morphology, crystallization, melting and biodegradation of poly(ε-caprolactone-co-ε-caprolactam) copolymers. Macromolecules 2009;42(17):6671–81.
[10] Chen X, Gonsalves KE, Cameron JA. Further studies on biodegradation of aliphatic poly(ester-amides). J Appl Polym Sci 1993;50(11):1999–2006.
[11] Müller A, Balsamo V, Arnal ML. Nucleation and crystallization in diblock and triblock copolymers. Adv Polym Sci 2005;190:1–63.
[12] Müller AJ, Arnal ML, Balsamo V. Crystallization in block copolymers with more than one crystallizable block. In: Reiter G, Strobl GR, editors. Progress in understanding of polymer crystallization. Berlin: Springer-Verlag; 2007. p. 229–59.
[13] Castillo RV, Müller AJ. Crystallization and morphology of biodegradable or biostable single and double crystalline block copolymers. Prog Polym Sci 2009;34(6):516–60.
[14] Loo YL, Register RA. Crystallization within block copolymer mesophases. In: Hamley IW, editor. Developments in block copolymer science and technology. New York: John Wiley & Sons, Inc.; 2004. p. 213–43.
[15] Hamley IW. The physics of block copolymers. Oxford: Oxford University Press; 1998.
[16] Deshayes G. Synthèse de nouveaux copolymères à blocs articulés sur des séquences polyesteramides. PhD Thesis, Faculty of Sciences, University of Mons-Hainaut; 2007.
[17] Santana OO, Müller AJ. Homogeneous nucleation of the dispersed crystallisable component of immiscible polymer blends. Polym Bull 1994;32(4):471–7.
[18] Arnal ML, Balsamo V, Ronca G, Sánchez A, Müller AJ, Cañizales E, et al. Applications of successive self-nucleation and annealing (SSA) to polymer characterization. J Therm Anal Calorim 2000;59(1–2):451–70.
[19] Müller AJ, Arnal ML. Thermal fractionation of polymers. Prog Polym Sci 2005;30(5):559–603.
[20] Lorenzo AT, Arnal ML, Müller AJ, Boschetti de Fierro A, Abetz V. High speed SSA thermal fractionation and limitations to the determination of lamellar sizes and their distributions. Macromol Chem Phys 2006;207(1):39–49.
[21] Müller AJ, Lorenzo AT, Arnal ML. Recent advances and applications of successive self-nucleation and annealing (SSA) high speed thermal fractionation. Macromol Symp 2009;277(1):207–14.
[22] Muller AJ, Hernandez Z, Arnal ML, Sanchez J. Successive self-nucleation/annealing (SSA): a novel technique o study molecular segregation during crystallization. Polym Bull 1997;39(4):465–72.
[23] Lorenzo A, Arnal ML, Albuerne J, Müller AJ. DSC isothermal polymer crystallization kinetics measurements and the use of the Avrami equation to fit the data: guidelines to avoid common problems. Polym Test 2007;26(2):222–31.
[24] Balsamo V, Urdaneta N, Pérez L, Carrizales P, Abetz V, Müller AJ. Effect of the polyethylene confinement and topology on its crystallisation within semicrystalline ABC triblock copolymers. Eur Polym J 2004;40(6):1033–49.
[25] Balsamo V, Müller AJ, Stadler R. Antinucleation effect of the polyethylene block on the polycaprolactone block in ABC triblock copolymers. Macromolecules 1998;31(22):7756–63.
[26] Sabino MA, Feijoo JL, Müller AJ. Crystallisation and morphology of neat and degraded poly(p-dioxanone). Polym Degrad Stab 2001;73(3):541–7.
[27] Mathot V. Calorimetry and thermal analysis of polymers. New York: Hanser Publishers; 1994.
[28] Schultz J. Polymer crystallization. Washington: Oxford University Press; 2001.
[29] Mardelkern L. Crystallization of polymer. Kinetics and mechanisms, vol. 2. Cambridge: Cambridge University Press; 2002.
[30] Strobl G. Crystallization and melting of bulk polymers: new observations, conclusions and a thermodynamic scheme. Prog Polym Sci 2006;31(4):398–442.
[31] Brandrup J, Immergut EH, Grulke EA, editors. Polymer handbook. New York: Wiley-Science; 1999.
[32] Marand H, Xu J, Srinivas S. Determination of the equilibrium melting temperature of polymer crystals: linear and nonlinear

Hoffman–Weeks extrapolations. Macromolecules 1998;31(23): 8219–29.
[33] Avrami M. Granulation, phase change, and microstructure kinetics of phase change. III. J Chem Phys 1941;9(2):177–84.
[34] He Y, Zhu B, Kai W, Inoue Y. Nanoscale-confined and fractional crystallization of poly(ethylene oxide) in the interlamellar region of poly(butylene succinate). Macromolecules 2004;37(9):3337–45.
[35] Mandelkern L. The crystalline state. In: Mark JE, editor. Physical properties of polymers. Cambridge: Cambridge University Press; 2004. p. 209–315.
[36] Strobl GA. Multiphase model describing polymer crystallization and melting. In: Reiter G, Strobl GR, editors. Progress in understanding of polymer crystallization. Lecture notes in physics, vol. 714. Germany: Springer; 2007. p. 481–502.
[37] Strobl G. From the melt via mesomorphic and granular crystalline layers to lamellar crystallites: a major route followed in polymer crystallization? Eur Phys J E 2000;3(2):165–83.
[38] Muthukumar M, Welch P. Modeling polymer crystallization from solutions. Polymer 2000;41(25):8833–7.
[39] Muthukumar M. Commentary on theories of polymer crystallization. Eur Phys J E 2000;3(2):199–202.
[40] Lorenzo AT, Müller AJ. Estimation of the nucleation and crystal growth contributions to the overall crystallization energy barrier. J Polym Sci B Polym Phys 2008;46(14):1478–87.
[41] Sperling LH. Introduction to physical polymer science. New Jersey: Wiley Interscience; 2006.
[42] Mark JE, editor. Physical properties of polymer handbook. New York: AIP Press; 1996.